Transient and steady-state amplitudes of forced waves in rectangular basins

D. F. Hill
Department of Civil and Environmental Engineering, The Pennsylvania State University, 212 Sackett Building, University Park, Pennsylvania 16802

(Received 10 May 2002; accepted 28 February 2003; published 5 May 2003)

A weakly-nonlinear analysis of the transient evolution of two-dimensional, standing waves in a rectangular basin is presented. The waves are resonated by periodic oscillation along an axis aligned with the wavenumber vector. The amplitude of oscillation is assumed to be small with respect to the basin dimensions. The effects of detuning, viscous damping, and cubic nonlinearity are all simultaneously considered. Moreover, the analysis is formulated in water of general depth. Multiple-scales analysis is used in order to derive an evolution equation for the complex amplitude of the resonated wave. From this equation, the maximum transient and steady-state amplitudes of the wave are determined. It is shown that steady-state analysis will underestimate the maximum response of a basin set into motion from rest. Amplitude response diagrams demonstrate good agreement with previous experimental investigations. The analysis is invalid in the vicinity of the ''critical depth'' and in the shallow-water limit. A separate analysis, which incorporates weak dispersion, is presented in order to provide satisfactory results in shallow water. © *2003 American Institute of Physics.* [DOI: 10.1063/1.1569917]

I. INTRODUCTION

A. Nonlinear standing waves

While studies of finite-amplitude effects can be traced back to Stokes,[1] for the case of progressive waves, a similar study of standing waves did not occur for another century. Penney and Price[2] formulated a weakly-nonlinear theory for standing waves in infinite depth and Tadjbakhsh and Keller[3] considered the more general case of arbitrary depth. The results for the standing wave case were found to be similar to the progressive wave case in the sense that the wave frequency became amplitude dependent and the free-surface profile distorted due to the presence of bound superharmonics. Of particular interest was the result that the sign of the frequency shift (from the linear value) depended upon the relative depth (ratio of depth to wavelength) of the water. Tadjbakhsh and Keller[3] found the critical value of this ratio to be equal to 0.17. Motivated by this work, Fultz[4] conducted an experimental study which confirmed the presence of this frequency reversal, but showed the critical value to be 0.14. In a multiple-scales, slowly-varying analysis of finite depth standing waves, Roskes[5] demonstrated that sideband instabilities would occur beyond a critical depth of 0.162, which is precisely the critical depth determined in the present study.

B. Parametric instability

The above studies focused on the characteristics of *free*, i.e., unforced, weakly-nonlinear standing waves, with little emphasis on the generation of the waves. Vertical oscillation, known as Faraday resonance, of a fluid domain, can generate subharmonic standing waves. Because the base state of the flow in this case is periodic, this type of instability is known as a parametric instability.[6] First observed by Faraday,[7] the rigorous explanation of this phenomenon was provided by Benjamin and Ursell.[8] Since then, theoretical and experimental studies of Faraday waves have significantly advanced the understanding of nonlinear standing waves. A detailed review is given by Miles and Henderson.[9]

Faraday resonance results in initial exponential growth of the forced wave. The inclusion of weak viscosity reduces the growth rate and establishes a minimum forcing amplitude necessary for growth.[10] If cubic nonlinearity is considered, it can be shown that the waves do not grow unbounded, but rather attain a maximum amplitude due to nonlinear frequency detuning. Generally speaking, an evolution equation of the form

$$\dot{a} = i\Delta a - i\beta a^* - (1-i)\alpha a - i\lambda a^2 a^* \tag{1}$$

is obtained, where a is a complex amplitude, and Δ, β, α, and λ are real-valued detuning, forcing, damping, and nonlinear interaction coefficients.

Investigations of Faraday resonance have not been limited only to surface water waves. For example, Foda and Tzang[11] and Kumar[12] both studied the Faraday resonance of thin viscoelastic layers. Umbanhowar *et al.*[13] have shown that Faraday resonance can excite three-dimensional standing ''waves'' in a pure granular medium as well. Finally, the Faraday resonance of interfacial waves has been pursued by many authors, including Benielli and Sommeria[14] and Hill.[15] The experimentally determined growth rates and maximum amplitudes of the former authors were found to agree well with the predictions of the latter author.

Parametric instabilities may also be driven by nonlinear interactions between modes. An elegant example is that of edge waves on sloping boundaries. These trapped modes

propagate in the alongshore direction and were shown by Guza and Davis[16] to be resonated by weakly nonlinear, normally incident surface waves. It has been hypothesized that edge waves resonated in this fashion play a role in generating the regularly spaced beach cusps that are found in many coastal areas. As with the case of Faraday resonance, a maximum resonated wave amplitude, which is much larger than the incident wave amplitude, can be determined. This third-order analysis has been performed by Guza and Bowen,[17] Minzoni and Whitham,[18] and Rockliff.[19]

C. Horizontal resonance

If a basin of fluid is oscillated horizontally, rather than vertically, waves can again be resonated, although there are some important differences. Generally speaking, an amplitude evolution equation of the form

$$\dot{a}=\beta+i\Delta a-(1-i)\alpha a-i\lambda a^2 a^*, \tag{2}$$

where Δ, β, α, and λ are as above, is now obtained. The initial growth is now linear in time and the effect of viscosity is to contribute to placing an upper bound on the wave amplitude rather than solely reducing the rate of growth.

There have been a number of studies in the past that have dealt with horizontal resonance. Chester[20] and Chester and Bones[21] included the effects of weak dispersion and weak viscosity in their theoretical and experimental studies of resonant waves. The individual roles played by nonlinearity, dispersion, and damping are summarized by the latter authors:[21]

> The leaning over of the curve near a local maximum...must be a nonlinear effect closely associated with ''hard spring'' solution of Duffing's equation. The existence of several maxima is the result of dispersion, and the fact that a maximum is actually attained and that the response curve is connected arises from dissipation.

The experimental data indicated that the number of bifurcation points in the amplitude response diagram was a decreasing function of the relative depth of the fluid. For example, experiments performed at identical forcing amplitudes yielded a response curve with six bifurcations when the relative depth was 0.042, but a curve with only three bifurcations when the depth was 0.083.

Lepelletier and Raichlen[22] used long-wave theory, also with dispersive and dissipative terms, and paid particular attention to the transients associated with the commencement and cessation of the basin motion. Their study gave an explicit result for the initial linear growth rate of the resonated wave. Solving the nonlinear problem numerically, the authors produced amplitude response diagrams that showed the same lean to the right as the studies listed above. Maximum amplitudes were found to be one to two orders of magnitude greater than the forcing amplitude and experiments were found to agree very well with the theory.

The work of Waterhouse[23] is significant in that it paid special attention to resonance at near-critical depths. Following the lead of Ockendon and Ockendon,[24] the problem was re-scaled to handle this special case. Prior to this, response curves[3,4] had demonstrated a transition from ''hard spring'' to ''soft spring'' behavior as the water depth had passed through the critical value. The re-scaling by Waterhouse[23] unified the two responses, illustrating that the shallow-water hard-spring behavior was, in actuality, a soft-spring response with an extra ''kink.'' As a result, a quintic equation in maximum amplitude was derived.

Finally, the important works of Faltinsen[25] and Faltinsen *et al.*[26] must be discussed, as they closely relate to the current analysis. In the former paper, the author used perturbation methods and inviscid analysis to derive a cubic equation governing the maximum wave amplitude in water of general depth. A solution of this equation yielded an amplitude response curve similar to those discussed above. The latter paper relaxed many of the assumptions of the former and used multi-dimensional modal analysis to analyze the transient behavior of the resonated waves. Damping was considered phenomenologically. Good agreement between theory and experiment was reported and many of the observations are consistent with the present analysis. Of particular note is the conclusion that, in large tanks, steady-state analysis is not particularly valuable. This is because (i) the maximum transient amplitude can far exceed the steady-state amplitude and (ii) the time that it takes to actually achieve a steady-state can far exceed the duration of the forcing.

D. Present analysis

The present analysis distinguishes itself from previous studies in that it simultaneously considers the effects of weak viscosity, general water depth, and transient wave evolution. Most previous studies focused only on steady-state analysis and did not describe the temporal evolution of the amplitude. Those that gave consideration to transient analysis[22,26] were numerical in nature, with only limited results being presented. By using a multiple-scales analysis, the present study yields an amplitude evolution equation with extremely compact coefficients. As a result, consideration of a wide range of parameter space is possible. Upon comparison with existing experimental studies, the present analysis is seen to perform well.

The present study also elaborates upon the difference between transient and steady-state amplitude response diagrams. In this context, ''transient'' refers to the maximum amplitude the system will obtain once set into motion from rest and ''steady-state'' refers to the fixed-point solution of the system. Upon comparison, it is seen that previous formulations[20,21] will underestimate the maximum response of a basin set into motion from a state of rest.

One potential application of the current study is to the prediction of seismically forced waves in lakes, reservoirs, and fluid storage containers. An understanding of the rate of growth and maximum amplitude of resonated waves will allow for a prediction of shoreline inundation, spillway overtopping, and dynamic loading. As an example, Ruscher[27] conducted experimental studies of a scale model of the Los Angeles Reservoir following the 1994 Northridge Earthquake. The results noted in particular the rich variety of modes that can be generated in seemingly simple geometries.

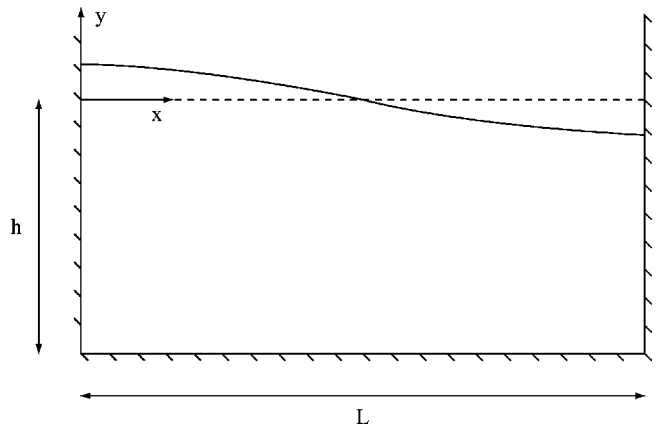

FIG. 1. Schematic of rectangular basin geometry. The basin length, breadth, and undisturbed depth are given by L, D, and h, respectively.

II. FORMULATION

As illustrated in Fig. 1, two-dimensional waves, of wavenumber k, in a basin of depth h and length L are considered. The breadth of the basin is D. The fluid density and kinematic viscosity are ρ and ν, respectively. Periodic forcing of the basin in the x direction is facilitated by prescribing the velocity of the $x=0$ and $x=L$ vertical walls to be

$$U_0 = U_L = \frac{b\omega}{2} e^{-i(\omega+\Delta)t} + \text{c.c.}, \tag{3}$$

where b is a real-valued displacement amplitude, ω is a linear resonant frequency of the basin, Δ is some small detuning from this resonant frequency, and c.c. denotes the complex conjugate.

The free-surface displacement is described by $\xi(x,t)$. If the fluid is assumed to be weakly-viscous, the velocity vector, $\mathbf{u}=(u,v,w)$, is given by the sum of the gradient of a potential function, $\Phi(x,y,t)$, which satisfies Laplace's equation,

$$\nabla^2\Phi = 0, \quad -h \leqslant y \leqslant \xi, \tag{4}$$

and a rotational velocity vector $\mathbf{U}=(U,V,W)$. By definition, therefore, $\boldsymbol{\nabla}\cdot\mathbf{U}=0$. Through a restriction to weak viscosity, the rotational velocity vector is only of significance in the vicinity of boundaries. A solution for these boundary layer corrections and their incorporation into the boundary value problem are discussed at length by Mei and Liu[28] and Mei[29] and will not be presented here.

The problem is to be solved subject to the familiar boundary conditions

$$\mathbf{u} = 0, \quad \text{all solid boundaries}, \tag{5}$$

$$g\xi + \Phi_t + \tfrac{1}{2}\mathbf{u}\cdot\mathbf{u} = 0, \quad y=\xi, \tag{6}$$

$$\xi_t + u\xi_x = v, \quad y=\xi. \tag{7}$$

Since cubic nonlinearity will be considered, the free surface boundary conditions are Taylor expanded about the undisturbed free surface, yielding

$$g\xi + \Phi_t = -\tfrac{1}{2}\mathbf{u}\cdot\mathbf{u} - \xi\Phi_{ty} - \tfrac{1}{2}\xi^2\Phi_{tyy} - \tfrac{1}{2}\xi[\mathbf{u}\cdot\mathbf{u}]_y, \quad y=0, \tag{8}$$

$$v - \xi_t = u\xi_x - \xi v_y - \tfrac{1}{2}\xi^2 v_{yy} + u_y\xi\xi_x, \quad y=0. \tag{9}$$

Next, the problem is to be solved at successive orders, based upon an expansion in a small parameter ϵ. In this case, the small parameter is formalized as the ratio of the forcing amplitude b to the tank length L. For cubic nonlinearity to balance the forcing, therefore, it is seen from (2) that $a \sim \epsilon^{1/3}$ is required. Additionally, both detuning and the slow time scale on which a evolves should scale by $\epsilon^{2/3}$. Finally, the viscosity of the fluid should scale by $\epsilon^{4/3}$. Thus, the problem may be nondimensionalized by adopting the following:

$$h^* = \frac{h}{L}, \quad D^* = \frac{D}{L}, \quad b^* = \frac{b}{\epsilon L} \equiv 1,$$

$$t^* = t\sqrt{g/L}, \quad \omega^* = \frac{\omega}{\sqrt{g/L}}, \quad \Delta^* = \frac{\Delta}{\epsilon^{2/3}\sqrt{g/L}},$$

$$a^* = \frac{a}{\epsilon^{1/3}L}, \quad \nu^* = \frac{\nu}{\epsilon^{4/3}L^2\sqrt{g/L}}, \quad \mathbf{u}^* = \frac{\mathbf{u}}{\epsilon^{1/3}L\sqrt{g/L}},$$

$$\xi^* = \frac{\xi}{\epsilon^{1/3}L}.$$

The asterisks are subsequently dropped and nondimensional quantities are understood. In the results section, some dimensional results will be presented to facilitate comparisons with previous studies. This will be clarified locally.

The free-surface displacement is taken to be

$$\begin{aligned}\xi = {} & \epsilon^{1/3}\eta_{01}\cos(n\pi x)e^{-i\omega t} + \epsilon^{2/3}\eta_{10} \\ & + \epsilon^{2/3}\eta_{12}\cos(2n\pi x)e^{-2i\omega t} + \epsilon\eta_{21}\cos(n\pi x)e^{-i\omega t} \\ & + \epsilon\eta_{23}\cos(3n\pi x)e^{-3i\omega t} + \text{c.c.},\end{aligned} \tag{10}$$

where n is the integer mode number of the wave. As indicated by this expansion, both a bound superharmonic and a set-down of the water surface are expected at second order. At third order, a bound superharmonic and a term in phase with the fundamental are expected. The expansion for the velocity potential is similar, with the exception that there is no equivalent set-down term.

At the leading order, there is only the well-known solution for the linear standing wave,

$$\eta_{01} = \frac{a}{2}, \tag{11}$$

$$\phi_{01} = \frac{-ia\omega}{2n\pi\sinh(n\pi h)}\cosh[n\pi(y+h)], \tag{12}$$

with $\omega^2 = n\pi\tanh(n\pi h)$.

At the next order, the familiar Stokes wave solution for the superharmonic is found:[3]

$$\eta_{12}=\frac{a^2 n\pi \cosh(n\pi h)}{16\sinh^3(n\pi h)}[2\cosh^2(n\pi h)+1], \tag{13}$$

$$\phi_{12}=\frac{-3i\omega a^2}{32\sinh^4(n\pi h)}\cosh[2n\pi(y+h)]. \tag{14}$$

The ''zeroth'' harmonic, i.e., the steady-state set-down of the water surface, is given by

$$\eta_{10}=\tfrac{1}{8}\omega^2|a|^2[1+\coth^2(n\pi h)]\cos(2n\pi x) - \frac{n\pi|a|^2}{4\sinh(2n\pi h)}. \tag{15}$$

Tadjbakhsh and Keller[3] derived the first term, which applies to standing waves only, but omitted the second term, which is well-known[29,30] and which applies to both progressive and standing waves.

Finally, at the third order, there are two problems to solve. The first is for the bound superharmonic η_{23}, whose free surface displacement is given by

$$\eta_{23}=\frac{3n^2\pi^2 a^3[1+8\cosh^6(n\pi h)]}{512[\cosh^6(n\pi h)-3\cosh^4(n\pi h)+3\cosh^2(n\pi h)-1]}. \tag{16}$$

Second, and of greater interest, an inhomogeneous problem for the fundamental harmonic is obtained. Because of the choice of scalings, the forcing, damping, detuning, and cubic nonlinearity all enter the problem at this order. Due to the existence of a nontrivial solution at leading order, it is necessary to impose an orthogonality condition on the homogeneous and inhomogeneous solutions to guarantee solvability.[31] Known as the Fredholm alternative, this application of Green's theorem leads directly to a temporal evolution equation for the wave amplitude:

$$\dot{a}=i\Delta a-(1-i)\alpha a+\beta-i\lambda|a|^2 a, \tag{17}$$

where the differentiation is with respect to the slow time scale τ.

In this equation, α is a damping coefficient, given by Keulegan[32] as

$$\alpha=\frac{1}{n\pi}\sqrt{\frac{\nu\omega}{2}}\left[\frac{1}{D}+1+\frac{n\pi(1-2h)}{\sinh(2n\pi h)}\right]. \tag{18}$$

It should be noted that this result is not exact, as it is based upon a boundary layer approximation and neglects damping in the bulk. Indeed, the measurements of Keulegan[32] differed significantly from (18) in the case of small, nonwetting (distilled water and lucite) basins. If the basin was large or wetting (glass), the differences were only slight. In both cases, the discrepancies were partly attributed to surface-tension and surface-contamination effects. Martel *et al.*[33] give a more complete treatment of damping, where the rate of energy dissipation in the bulk is included. Given the small volume to surface area ratio of their experiments on capillary waves, this was warranted. Given the large volume to surface area ratio of the experiments discussed in Sec. III A, this level of detail is unwarranted in the present analysis. Moreover, within the formal framework of the current perturbation approach and the chosen scaling of the viscosity, damping in the bulk does not enter the problem until an order higher than what is being considered. Thus, the use of (18) is justified.

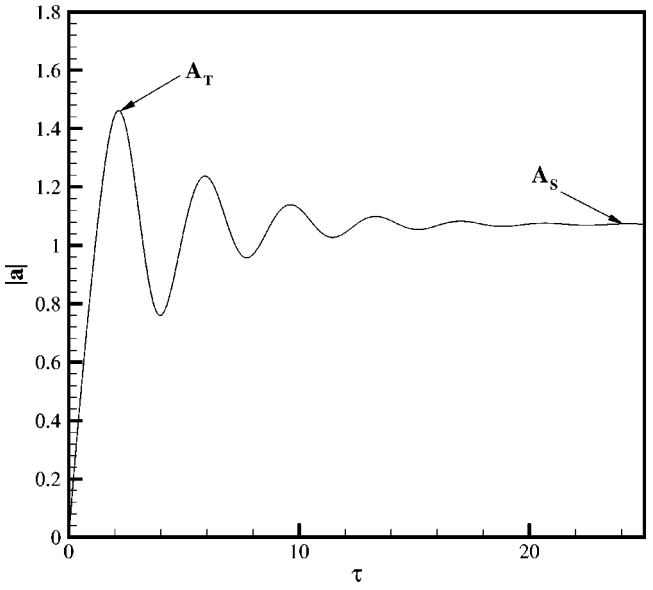

FIG. 2. Temporal evolution of wave amplitude $|a|$, obtained from (21)–(22) for the case of $\alpha=0.25$, $\beta=1$, $\lambda=1$, and $\Delta=0$.

The forcing coefficient β is given by

$$\beta=[1+(-1)^{n-1}]\frac{1}{\sqrt{n\pi}}[\tanh(n\pi h)]^{3/2}, \tag{19}$$

and the nonlinear interaction coefficient λ is given by

$$\lambda=\frac{\omega n^2\pi^2}{256\sinh^4(n\pi h)\cosh^2(n\pi h)}[-\cosh(6n\pi h) + 6\cosh(4n\pi h)+24+7\cosh(2n\pi h)]. \tag{20}$$

Setting $\lambda=0$ reveals the critical depth to be 0.162. Note as well that λ is a monotonically decreasing function of both h and n and that $\lambda\to\infty$ as $h\to 0$, indicating the invalidity of the solution in shallow water.

Noting that the complex amplitude a can be expressed as its amplitude and phase, i.e., $a=|a|e^{i\theta}$, (17) is decomposed into the coupled equations,

$$\frac{d|a|}{d\tau}=\beta\cos\theta-\alpha|a|, \tag{21}$$

$$|a|\frac{d\theta}{d\tau}=-\beta\sin\theta+(\Delta+\alpha)|a|-\lambda|a|^3. \tag{22}$$

As an example, Fig. 2 shows the evolution of the amplitude $|a|$ with τ for the case of $\alpha=0.25$, $\beta=1$, $\lambda=1$, and $\Delta=0$. Clearly evident are the maximum transient amplitude A_T and the steady-state amplitude A_S.

III. RESULTS

Before considering the nonlinear results, there are a few interesting points to make. First of all, note that, from a state

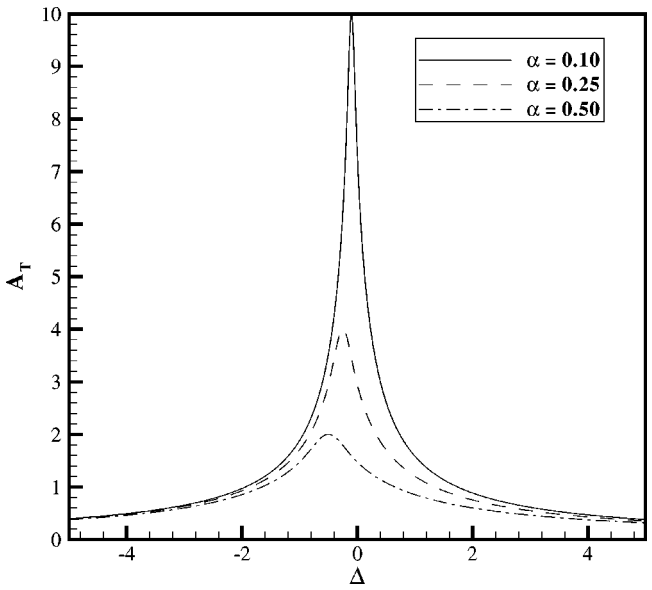

FIG. 3. Transient amplitude response diagrams, obtained from (23), for the case of $\beta=1.0$. The different curves denote different amounts of damping.

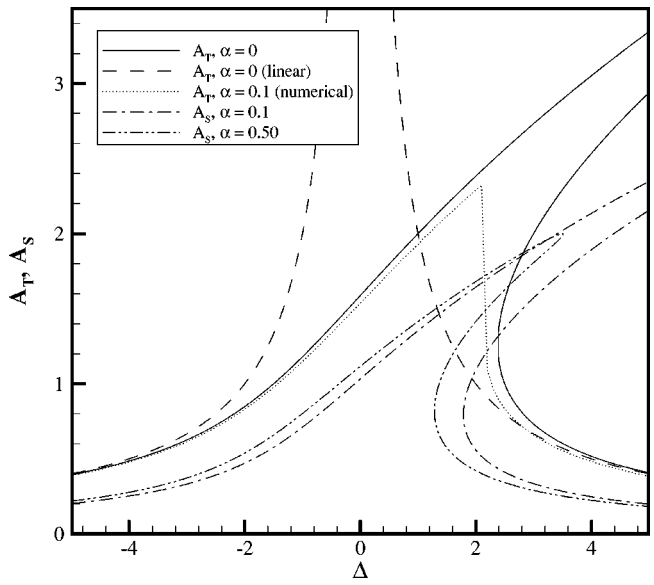

FIG. 4. Transient and steady-state amplitude response diagrams, as predicted by nonlinear theory (25), (28). Also shown are sample transient results from numerical integration of the nonlinear equation (17) and sample transient results from linear theory (23). $\beta=1.0$ for all curves and $\lambda=1.0$ for all nonlinear curves. Damping values are specified in the legend.

of rest, no growth ($\beta=0$) is predicted for even modes. This is because the horizontal forcing is anti-symmetric and two-dimensional waves with even mode numbers are symmetric.[34]

Next, if the linear limit is considered ($\lambda=0$), it is straightforward to derive expressions for the maximum transient and steady-state amplitudes:

$$A_T=\frac{\beta}{[\alpha^2+(\Delta+\alpha)^2]^{1/2}}\left[1+\exp\left(-\frac{2\alpha\pi}{|\alpha+\Delta|}\right)+2\exp\left(-\frac{\alpha\pi}{|\alpha+\Delta|}\right)\right]^{1/2}, \tag{23}$$

$$A_S=\frac{\beta}{[\alpha^2+(\Delta+\alpha)^2]^{1/2}}, \tag{24}$$

which, in the inviscid limit, become $A_T=2\beta/\Delta$ and $A_S=\beta/\Delta$.

Figure 3 shows the variation of A_T with Δ and α for a fixed value of β. The steady-state amplitude response curves are similar in shape. From (23)–(24), it is clear that when $\Delta=-\alpha$, $A_S=A_T$ and when $|1+\Delta/\alpha|\gg 1$ or $\alpha\to 0$, $A_S\to A_T/2$. Similar response curves were shown by Lepelletier and Raichlen,[22] minus the frequency shift due to viscosity.

Of much greater interest is the response when nonlinearity is included. Considering first the steady-state response, the derivatives in (21)–(22) are set to zero and the equations are subsequently squared and added to yield

$$|a|^6-\frac{2(\Delta+\alpha)}{\lambda}|a|^4+\frac{\alpha^2+(\Delta+\alpha)^2}{\lambda^2}|a|^2-\frac{\beta^2}{\lambda^2}=0. \tag{25}$$

This equation, which is cubic in $|a|^2$, is easily solved (e.g., Abramowitz and Stegun[35]) to obtain the response diagram for A_S. For nonzero α, there are two bifurcation points. In the inviscid limit, the single bifurcation point is easily shown to be at

$$\Delta=\left[\frac{27\lambda\beta^2}{4}\right]^{1/3}. \tag{26}$$

The transient response is more difficult to obtain analytically, in the case of general α. However, as will be illustrated in Sec. III A, it turns out that $\alpha\ll 1$ for water waves in large tanks. As a result, the damping in this case has little role in determining A_T and it is reasonable to deduce a transient response diagram for the inviscid limit. To do this, (21)–(22) are first divided and then rearranged to take the form of a perfect differential. Integrating, it is seen that the quantity

$$\beta|a|\sin\theta-\tfrac{1}{2}\Delta|a|^2+\tfrac{1}{4}\lambda|a|^4 \tag{27}$$

is a constant of the motion.

Next, if the basin is being set into motion from a state of rest ($|a|=0$), it follows that the constant is zero for all times. Finally, when $|a|$ reaches a local maximum, the inviscid limit of (21) shows that $\theta=\pm\pi/2$. Thus, the equation

$$|a|^3-\frac{2\Delta}{\lambda}|a|\pm\frac{4\beta}{\lambda}=0 \tag{28}$$

may be solved exactly to obtain A_T. The single bifurcation point of the transient response occurs at

$$\Delta=\left[\frac{27\lambda\beta^2}{2}\right]^{1/3}. \tag{29}$$

Figure 4 shows the variation of A_S, as obtained from (25), with α and Δ for fixed values of β and λ. In this case $\lambda>0$, so the water is relatively shallow (i.e., less than the "critical" depth). As the damping increases, there is a slight migration of the response curve to the left and, more pronounced, the two bifurcation points tend towards one an-

other. Note that the second bifurcation point is within the graph axes only for the $\alpha=0.5$ case. At large enough values of α, the bifurcation points vanish altogether and the amplitude response becomes single-valued for all Δ. For the current example, this occurs when $\alpha=0.86$.

Also shown, for the sake of comparison, are the undamped transient response curves, obtained from (23) and (28). The former is included in order to highlight the inadequacy of the linear theory near resonance. Note that while (28) predicts three possible amplitudes at values of detuning beyond the bifurcation point, the two highest amplitudes are spurious. This is because, in addition to the initial condition $|a|=0$ that was used in deriving (28), there are other combinations of nonzero $|a|$ and θ that result in (27) being zero. Finally, the damped ($\alpha=0.1$) transient response curve, obtained by numerically integrating (17) from the initial condition $a=0$, is also shown. A fourth-order explicit Runge–Kutta scheme, utilizing the Dormand–Prince pair,[36] was used to carry out the integration and, as alluded to earlier, the omission of weak damping in (28) leads to only a slight overestimation of A_T. Note also the "jump" to the lower branch of the numerically-obtained transient response diagram with increasing Δ.

Further insight into the steady-state and transient solutions shown in Fig. 4 can be gained by introducing $u=|a|\cos\theta$ and $v=|a|\sin\theta$, in which case the constant given in (27) becomes

$$\beta v-\tfrac{1}{2}\Delta(u^2+v^2)+\tfrac{1}{4}\lambda(u^2+v^2)^2. \tag{30}$$

Figure 5 shows contours of this constant for $\beta=1$, $\lambda=1$, $\Delta=1$, 2, 3. Recall as well that $\alpha=0$ was assumed in obtaining (27) and, therefore, (30). In the case of $\Delta=1$, there is a single, stable steady-state solution, as was shown in Fig. 4. Tracing the zero contour from the initial condition of $u=v=0$, it is clear that the maximum transient response exceeds the steady state. In the case of $\Delta=2$, there are two stable steady-state solutions, corresponding to the maximum and minimum roots of (25), and one unstable solution. Consideration of the contour passing through the origin reveals that the maximum transient response exceeds all of the steady-state values. Finally, in the case of $\Delta=3$, there are again two stable steady-state solutions and one unstable steady-state solution. While Fig. 4 suggests that there should be three possible solutions for A_T at this value of detuning, recall that the two largest solutions are spurious. This is evident when the contour passing through the origin is considered. Comparing Figs. 5(b)–5(c), it is clear that the zero contour has "pinched off," leading to the dramatic jump to the lowest branch of the transient response diagram, as was observed in the numerical results in Fig. 4.

An additional point of significant interest is under what conditions the linear and the nonlinear theories diverge. Recalling Fig. 4, the linear and nonlinear transient response diagrams were nearly coincident at large values of detuning. Figure 6 shows, in gray, the regions of validity of the linear theory for multiple values of α and λ. Here, validity is defined by the arbitrary criterion that the linear prediction be within $\pm 10\%$ of the nonlinear prediction. Regions that are white indicate linear predictions that are more than 10% above the nonlinear predictions and regions that are black indicate linear predictions that are more than 10% below the nonlinear predictions.

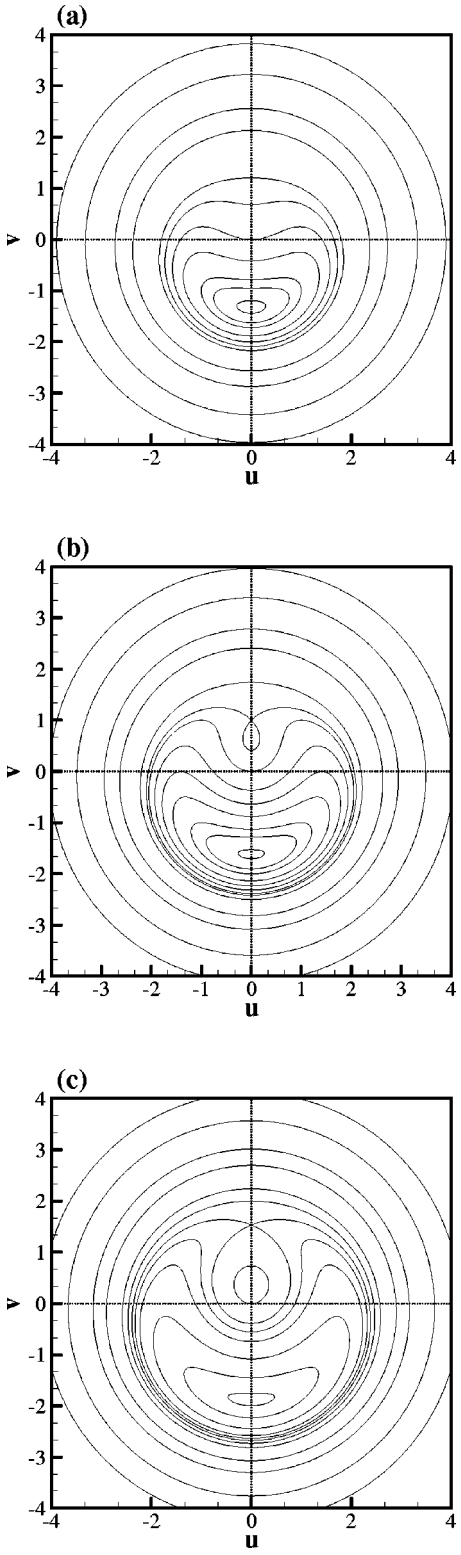

FIG. 5. Phase-plane diagrams of (30) for $\beta=1$ and $\lambda=1$. Note that (30) was derived assuming $\alpha=0$. (a) $\Delta=1$; (b) $\Delta=2$; (c) $\Delta=3$. In (a), one stable steady-state exists while in (b) and (c), two stable and one unstable steady-states exist. Tracing the contour that passes through the origin reveals the maximum transient that occurs in a basin excited from rest.

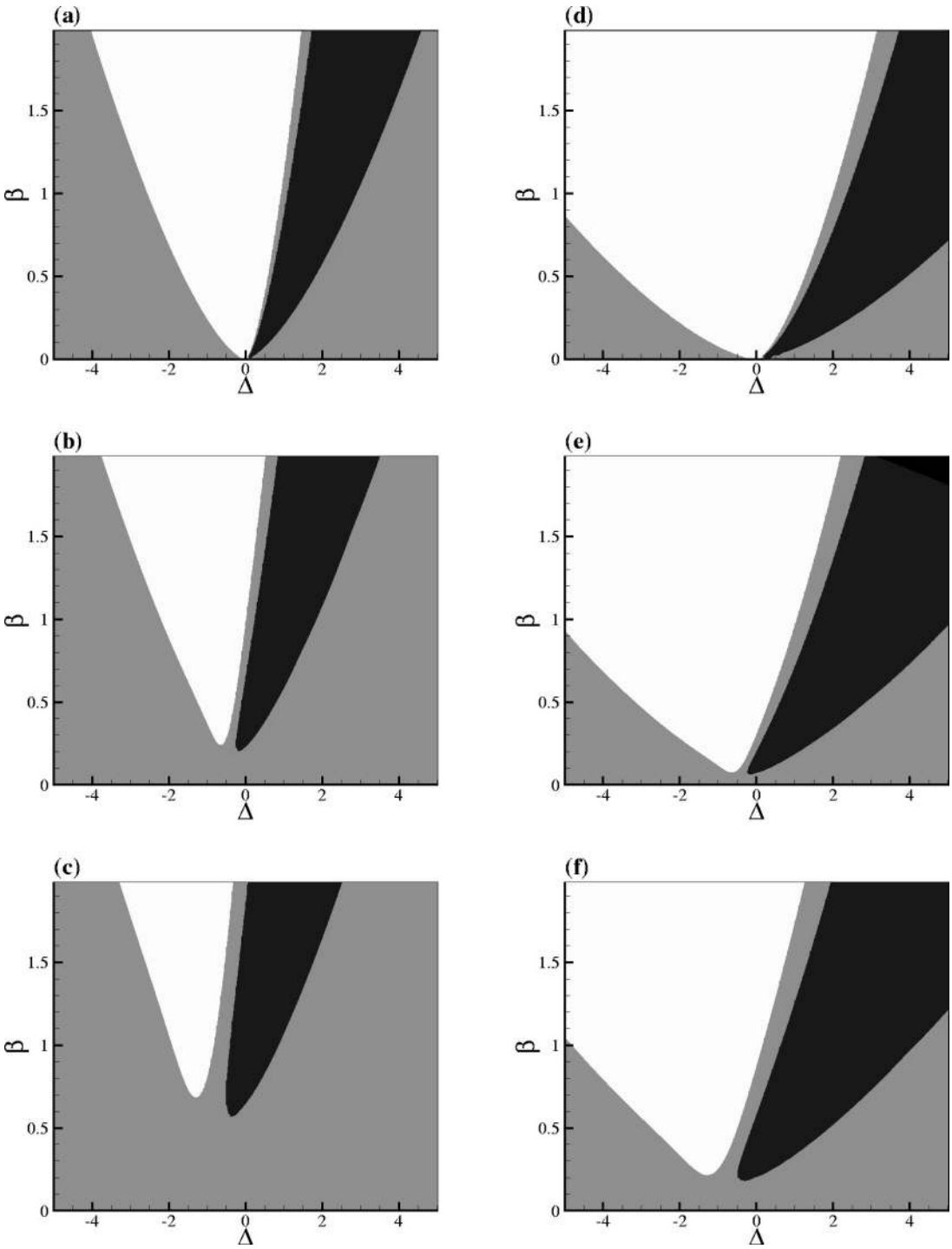

FIG. 6. An illustration of the range of validity of the linear theory. Gray denotes regions where linear predictions of A_T are within $\pm 10\%$ of nonlinear predictions of A_T. White regions indicate linear predictions that are more than 10% greater than nonlinear predictions and black regions indicate linear predictions that are more than 10% below the nonlinear predictions. (a) $\lambda=1$, $\alpha=0$; (b) $\lambda=1$, $\alpha=0.5$; (c) $\lambda=1$, $\alpha=1$; (d) $\lambda=10$, $\alpha=0$; (e) $\lambda=10$, $\alpha=0.5$; (f) $\lambda=10$, $\alpha=1$.

Consider first the undamped ($\alpha=0$) moderately nonlinear ($\lambda=1$) case shown in (a). First, it is clear, and intuitive, that as the system is forced harder, the detuning band where the linear theory is invalid increases. More interesting is the change in behavior with Δ at a fixed value of β. If the specific value of $\beta=1$ is considered, the conditions are the same as the inviscid transient curve in Fig. 4. At large negative values of Δ, the linear response is limited by the detuning, yielding amplitudes consistent with the nonlinear theory. As Δ approaches 0, the ''hard-spring'' nature of the nonlinear response results in the linear theory over-predicting the amplitudes. As Δ becomes positive, the two response curves cross, leading to a brief band of agreement before the linear theory begins, severely under-predicting the response. Finally, when the nonlinear response ''jumps'' down to the lower branch of the response curve, the two theories are

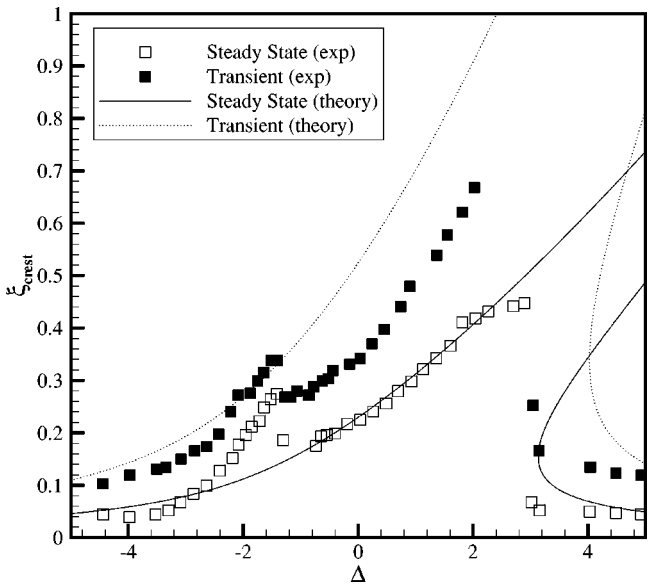

FIG. 7. A comparison between the present theory and the experimental data of Lepelletier and Raichlen (Ref. 22). Both transient and steady-state amplitude response diagrams are shown. $\alpha=0.0605$, $\beta=0.185$, $\lambda=141$, $\epsilon=0.00322$.

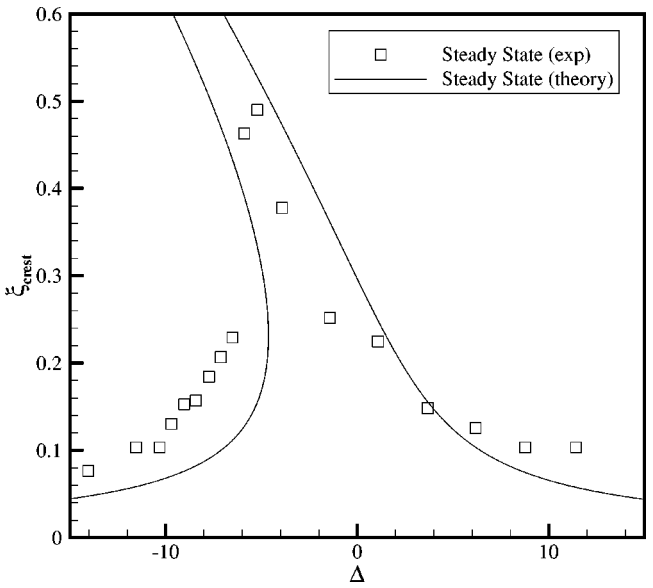

FIG. 8. A comparison between the present theory and the experimental data of Feng (Ref. 34). Only steady-state amplitude response diagrams are shown. $\alpha=0.0808$, $\beta=0.651$, $\lambda=-34.0$, $\epsilon=0.000656$.

again brought into agreement. The other plots in Fig. 6 illustrate that, as damping increases, the range of applicability of the linear theory broadens while, as nonlinearity increases, the range obviously narrows.

A. Comparison with experiments

Figure 7 shows the predictions of the present analysis, along with the experimental measurements of Lepelletier and Raichlen.[22] The dimensional parameters for this dataset are $L=0.6095$ m, $D=0.23$ m, $h=0.06$ m, $b=1.96\times10^{-3}$ m, $\nu=9.4\times10^{-7}$ m^2 s^{-1}, and $n=1$. The relative depth is therefore 0.0492. The corresponding nondimensional parameters are $\alpha=0.0605$, $\beta=0.185$, $\lambda=141$, and $\epsilon=0.00321$. The experimental results have been converted to the present nondimensional convention. Note that the vertical axis indicates the maximum crest elevations, not the maximum values of A_T and A_S.

Considering first the steady-state results, the agreement is quite good. The theory correctly predicts the major bifurcation at $\Delta\sim3.1$, but is unable to predict the dispersion-associated bifurcation at $\Delta\sim-1.5$. This clearly shows the inability of the present analysis to treat resonance in the shallow water limit.

With regards to the transient results, the agreement is reasonable, but it is clear that the theory consistently overpredicts the free-surface elevation and fails to correctly predict the location of the major bifurcation. Portions of the discrepancy can be attributed to the shallowness of the basin and the omission of viscosity in deducing the transient response diagram, as was illustrated in Fig. 4. A possible explanation for part of the balance of the discrepancy is offered by Faltinsen *et al.*[26] They note that the maximum transient amplitude is quite sensitive to initial conditions. They found that very slight motions existing in the tank at the commencement of an experiment could lead to values of A_T that were $\sim10\%$ different those predicted with the assumption, which was used in deriving (28), of zero initial conditions.

Some data on experiments in water of greater relative depth are provided by Feng.[34] The reported dimensional parameters are $L=0.2286$ m, $D=0.127$ m, $h=0.104$ m, and $n=3$. The relative depth is therefore 0.67. The kinematic viscosity was not reported and is assumed to be 1×10^{-6} m^2 s^{-1}. Regarding the forcing amplitude, the author controlled his tank with a function generator. The unfortunate aspect of this is that, as the forcing frequency was varied, so was the forcing amplitude. The only reference to the actual amplitude of oscillation is a statement that "the peak-to-peak amplitude of the moving platform...is about 0.3 mm." Assuming, therefore, that $b=0.15$ mm, the nondimensional parameters are $\alpha=0.0808$, $\beta=0.651$, $\lambda=-34.0$, and $\epsilon=0.000656$. As shown in Fig. 8, the agreement between the observations and the theory is reasonable, although large discrepancies exist at low forcing frequencies. More accurate information about the forcing amplitudes is needed to further investigate this discrepancy.

Additional experiments were conducted by Faltinsen *et al.*[26] Note that, in the following comparison, the variables are assumed to be dimensional, so as to facilitate comparison with reproduced figures. In their study, first-mode oscillations of a tank 1.73 m in length and 0.2 m in breadth were considered. The water depth was 0.6 m, yielding a relative depth of 0.173. While the authors do not present amplitude response diagrams, they do provide transient records of free-surface elevation at the tank end-wall.

Figure 9 shows the initial evolution of the free-surface displacement at the tank end-wall for two different values of detuning. For each case, the measurements and calculations of Faltinsen *et al.*[26] are shown, along with the calculations of the present study. In the first case, $b=3.2$ cm and $\Delta=0.424$ rad s^{-1}. The corresponding nondimensional param-

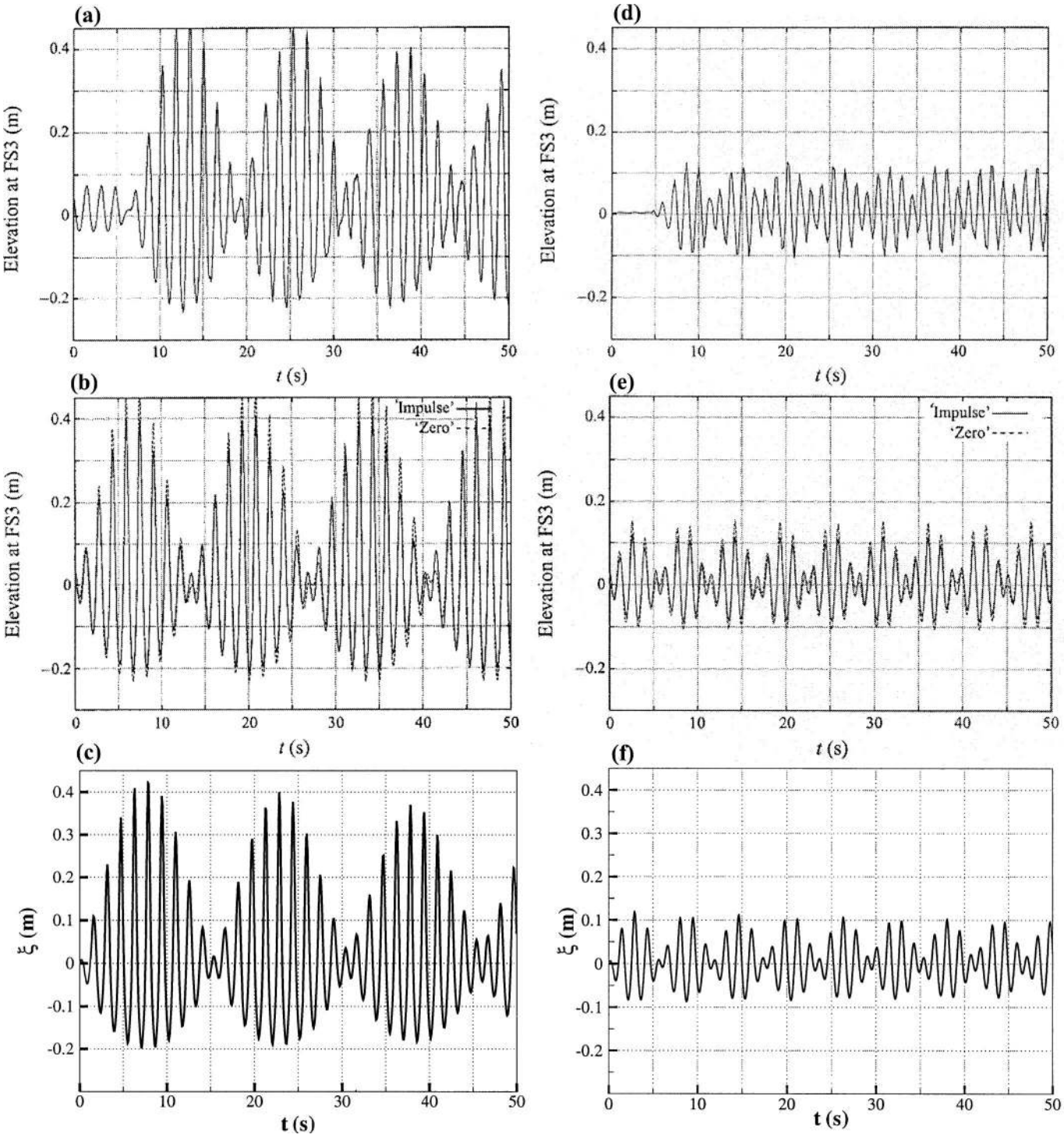

FIG. 9. A comparison of end-wall free-surface displacement between (a) the measurements of Faltinsen *et al.* (Ref. 26); (b) the calculations of Faltinsen *et al.* (Ref. 26), and (c) the calculations of the present study. Note that this figure presents results in dimensional format. $L=1.73$ m, $D=0.2$ m, $h=0.6$ m, $b=3.2$ cm, $n=1$, $\Delta=0.424$ rad s^{-1}, $\nu=1\times10^{-6}$ m^2 s^{-1}. Portions (d), (e), and (f) are similar, but with $b=2.9$ cm and $\Delta=1.07$ rad s^{-1}. Portions (a), (b), (d), and (e) reproduced with permission from Cambridge University Press.

eters are $\epsilon=0.0185$, $\alpha=0.015$, $\beta=0.453$, $\Delta=2.55$, and $\lambda=-0.409$. In the second case, $b=2.9$ cm and $\Delta=1.07$ rad s^{-1}. The corresponding nondimensional parameters are $\epsilon=0.0168$, $\alpha=0.0160$, $\beta=0.453$, $\Delta=6.83$, and $\lambda=-0.409$.

Note first of all that, in both experimental runs, the basin was not set into motion until $t\sim6$ s, hence the lack of synchronization between the observations and the calculations. For both experimental cases, the present analysis, which is extremely compact, performs very well in terms of predicting the maximum free-surface elevation. The present analysis correctly predicts the period of the nonlinear "beating" to be ~6 s in the case of $\Delta=1.07$ rad s^{-1}, but somewhat overestimates the period at ~15 s for the case of Δ

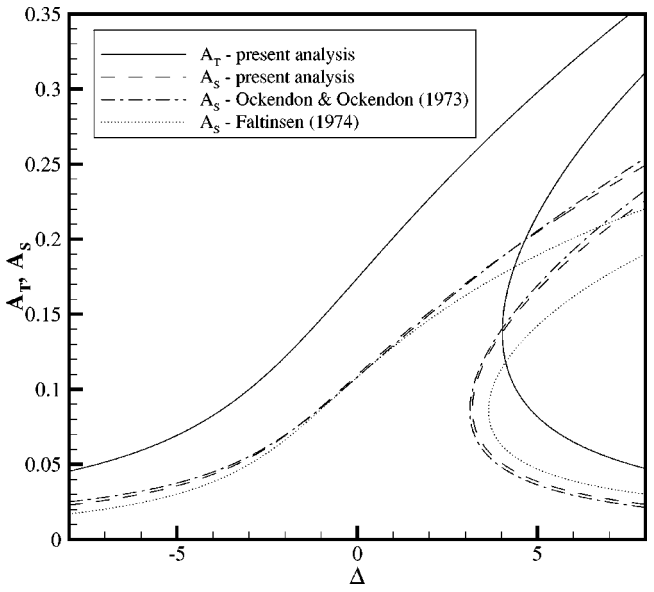

FIG. 10. A comparison of amplitude response diagrams obtained from the present transient theory (28), the present steady-state theory (25), the theory of Ockendon and Ockendon (Ref. 24), and the theory of Faltinsen (Ref. 25). $\alpha=0$, $\beta=0.185$, $\lambda=141$, $\epsilon=0.00322$.

$=0.424$ rad s^{-1}. The observations and calculations of Faltinsen *et al.*[26] show the period to be closer to 13 s.

B. Comparison with existing theories

As discussed in Sec. I C, there have been many previous theoretical studies of forced waves in tanks. It is therefore worthwhile to highlight the distinctions between those works and the present study. For example, consider the results of Ockendon and Ockendon[24] and Faltinsen.[25] Both approaches were inviscid investigations of the steady-state response of an oscillating tank.

As shown in Fig. 10, the steady-state predictions of both Ockendon and Ockendon[24] and Faltinsen[25] are very nearly identical to those predicted by (25) with $\alpha=0$. Since, as suggested by the data in Fig. 7, transient amplitudes can far exceed steady-state amplitudes, an application of these previous theories will underestimate the maximum amplitude in a basin set into motion from a state of rest. Another shortcoming of steady-state analysis is that, as pointed out by Faltinsen,[26] it can take an inordinate amount of time for a weakly-damped system to attain a fixed-point solution.

IV. SHALLOW WATER

As is well known and as pointed out by Faltinsen,[26] theories formulated in general depth fail in shallow water. Quadratic self-interactions of the fundamental mode will result in higher harmonics evolving on a slow time scale, rather than being bound. Thus, the problem must be reformulated, following the lead of Mei and Unluata.[37] Note that the formulation in this section is presented in a dimensional format. Using the shallow water equations,

$$\xi_t+hu_x+\xi u_x+u\xi_x=0, \tag{31}$$

$$u_t+uu_x+g\xi_x+\tfrac{1}{3}h^2u_{xxt}=0, \tag{32}$$

the free-surface displacement and horizontal velocity are expanded as

$$\xi=\sum_{q=1}^{n}\frac{a_q}{2}\cos(qkx)e^{-qi(\omega+\Delta)t}, \tag{33}$$

$$u=\sum_{q=1}^{n}\frac{i\omega a_q}{2kh}\sin(qkx)e^{-qi(\omega+\Delta)t}, \tag{34}$$

where n now refers to the number of modes retained and the complex conjugate is once again understood.

If weak detuning, viscosity, nonlinearity, and dispersion are all considered simultaneously, the following evolution equation for the qth mode is obtained:

$$\begin{aligned}\dot a_q=&\left[qi\Delta+\frac{i(q\omega)^3h}{6g}-(1-i)\sqrt{\frac{q\nu\omega}{2}}\frac{2h+D}{2hD}\right]a_q\\&-\frac{3i\omega}{8h}\left[\frac{q}{2}a_{q/2}^2+q\sum_{p=1}^{n-q}a_p^*a_{p+q}\right.\\&\left.+q\sum_{p=1}^{q/2-1}a_pa_{q-p}\right],\quad q\ \text{even};\\ \dot a_q=&\,\delta_{1q}\frac{2b\omega h}{L}+\left[qi\Delta+\frac{i(q\omega)^3h}{6g}-(1\right.\\&\left.-i)\sqrt{\frac{q\nu\omega}{2}}\frac{2h+D}{2hD}\right]a_q-\frac{3i\omega}{8h}\left[q\sum_{p=1}^{n-q}a_p^*a_{p+q}\right.\\&\left.+q\sum_{p=1}^{(q+1)/2-1}a_pa_{q-p}\right],\quad q\ \text{odd};\end{aligned} \tag{35}$$

where δ is the Kronecker delta. As an example, if seven modes are retained, the evolution equation for the primary $(q=1)$ mode is given by

$$\begin{aligned}\dot a_1=&\frac{2b\omega h}{L}+\left[i\Delta+\frac{i\omega^3h}{6g}-(1-i)\sqrt{\frac{\nu\omega}{2}}\frac{2h+D}{2hD}\right]a_1\\&-\frac{3i\omega}{8h}[a_1^*a_2+a_2^*a_3+a_3^*a_4+a_4^*a_5+a_5^*a_6\\&+a_6^*a_7].\end{aligned}$$

While the techniques that led to (25) and (28) could, in principle, be applied here to obtain coupled equations for the transient and steady-state solutions, it is more expedient to integrate the evolution equations numerically from the initial condition of $a_1=a_2=\cdots=a_n=0$. As in Sec. III, a fourth-order explicit Runge–Kutta scheme is used to carry out the integration. As an example, Fig. 11 shows the transient amplitude response curves for primary-mode resonance in a shallow basin ($L=117.5$ cm, $D=12$ cm, $h=6$ cm, $b=3.9$ mm, $\nu=9.4\times10^{-7}$ m^2 s^{-1}), as computed from the general-depth and the shallow-water theories. For comparison, the data of Lepelletier and Raichlen[22] are shown as well. Note that the dimensional results are plotted in a nondimen-

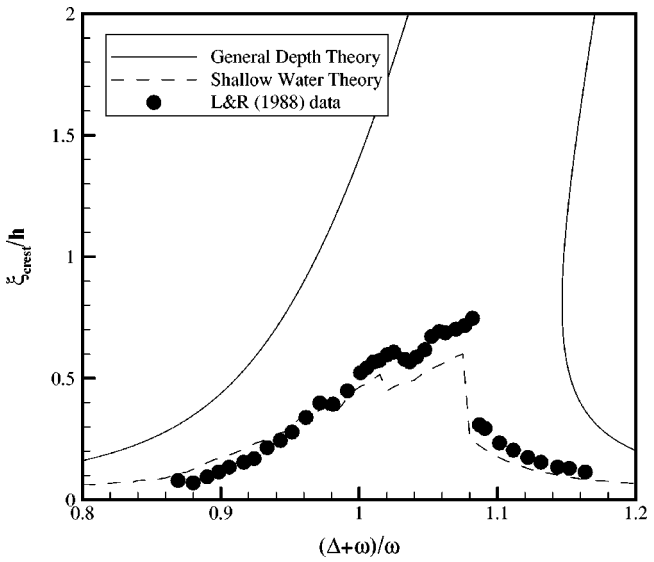

FIG. 11. A comparison between the general-depth and shallow-water transient amplitude response diagrams. $L=117.5$ cm, $D=12$ cm, $h=6$ cm, $b=3.9$ mm, $\nu=9.4\times10^{-7}$ m^2 s^{-1}. The data of Lepelletier and Raichlen (Ref. 22) are also shown.

sional format consistent with Lepelletier and Raichlen.[22] It is clear that the general-depth theory (28) is inadequate, as it massively over-predicts the response. However, the shallow-water approach outlined above, with seven modes retained, does a very good job of reproducing the observations. Not only are the amplitudes well predicted, but the major bifurcation point $((\Delta+\omega)/\omega\sim1.08)$ and both minor bifurcation points (~0.97, 1.02) are captured by the theory. For recent and much more detailed work on the transient response of shallow basins, the reader is referred to Faltinsen.[38]

V. CONCLUDING REMARKS

The conclusions of the present study can be summarized as follows. First, steady-state analysis has, with some slight differences, reproduced the theoretical amplitude response predictions of previous investigations. It was shown that the inclusion of viscosity is of minor consequence for large basins. In the inviscid limit, an extremely simple expression for the bifurcation frequency was found. The theory was found to compare reasonably well with existing experimental data in both shallow and deep water.

Second, transient analysis, which has received only limited attention previously, has been pursued and has revealed several interesting results. First of all, as with the steady-state response, it was shown that weak damping plays little role in determining the maximum response. Next, a comparison of the transient and steady-state amplitude response curves showed that the maximum response of a basin set into motion from rest can far exceed the steady-state response of the basin. In the analysis of a reservoir or storage container during a shaking event of finite duration, this may be of significance in terms of overtopping potential or ceiling impact. Finally, the bifurcation point of the transient response was found to occur at a larger (by a factor of $2^{1/3}$) value of detuning than the steady-state response.

Third, the theory, as formulated in water of arbitrary depth, is invalid at the critical depth and is also invalid in very shallow water. By revisiting the analysis with the shallow-water Boussinesq equations and retaining a sufficient number of modes, it was shown that good agreement with experiments in shallow water could be obtained. In particular, the additional bifurcation frequencies associated with dispersion were shown to be captured by the shallow-water theory.

In closing, the differences between the transient and steady-state responses raise some interesting questions that could be answered by future experimentation. Of particular interest is the hysteretic behavior that is observed in steady-state response diagrams when experiments are performed by scanning through forcing frequencies both forwards and backwards. When scanning along the lower branch, there is a jump to the upper branch in the vicinity of (26). Scanning in the opposite direction along the upper branch, however, results in a jump to the lower branch at a detuning value of greater magnitude. In light of the presence of an additional bifurcation frequency (29) associated with transient motion, and the lack, to the author's knowledge, of any published experiments on the matter, it would be interesting to investigate the experimental location of this second jump. Also of interest is the question of whether steady-state response curves obtained in a continuous experiment, where the frequency is incrementally adjusted, are identical to those obtained in a series of experiments at different frequencies, each beginning from rest.

ACKNOWLEDGMENTS

The author would like to thank Dr. Joseph Cusumano for helpful discussions regarding the transient amplitude response curves.

[1] G. G. Stokes, "On the theory of oscillatory waves," Trans. Cambridge Philos. Soc. **8**, 441 (1847).
[2] W. G. Penney and A. T. Price, "Some gravity wave problems in the motion of perfect liquids. Part II. Finite periodic stationary gravity waves in a perfect liquid," Philos. Trans. R. Soc. London, Ser. A **244**, 254 (1952).
[3] I. Tadjbakhsh and J. B. Keller, "Standing surface waves of finite amplitude," J. Fluid Mech. **8**, 442 (1960).
[4] D. Fultz, "An experimental note on finite-amplitude standing gravity waves," J. Fluid Mech. **13**, 193 (1962).
[5] G. J. Roskes, "Nonlinear slowly varying finite depth standing waves," Phys. Fluids **28**, 998 (1985).
[6] P. G. Drazin and W. H. Reid, *Hydrodynamic Stability* (Cambridge University Press, Cambridge, 1981).
[7] M. Faraday, "On a peculiar class of acoustical figures: and on certain forms assumed by groups of particles upon vibrating elastic surfaces," Philos. Trans. R. Soc. London **121**, 299 (1831).
[8] T. B. Benjamin and F. Ursell, "The stability of the plane free surface of a liquid in vertical periodic motion," Proc. R. Soc. London **225**, 505 (1954).
[9] J. Miles and D. Henderson, "Parametrically forced surface waves," Annu. Rev. Fluid Mech. **22**, 143 (1990).
[10] D. M. Henderson and J. W. Miles, "Single-mode Faraday waves in small cylinders," J. Fluid Mech. **213**, 95 (1990).
[11] M. A. Foda and S.-Y. Tzang, "Resonant fluidization of silty soil by water waves," J. Geophys. Res. **99**, 20463 (1994).
[12] S. Kumar, "Parametrically driven surface waves in viscoelastic liquids," Phys. Fluids **11**, 1970 (1999).
[13] P. B. Umbanhowar, F. Melo, and H. L. Swinney, "Localized excitations in a vertically vibrated granular layer," Nature (London) **382**, 793 (1996).
[14] D. Benielli and J. Sommeria, "Excitation and breaking of internal gravity

waves by parametric instability,'' J. Fluid Mech. **374**, 117 (1998).
[15]D. F. Hill, ''The Faraday resonance of interfacial waves in weakly viscous fluids,'' Phys. Fluids **14**, 158 (2002).
[16]R. T. Guza and R. E. Davis, ''Excitation of edge waves by waves incident on a beach,'' J. Geophys. Res. **79**, 1285 (1974).
[17]R. T. Guza and A. J. Bowen, ''Finite amplitude edge waves,'' J. Mar. Res. **34**, 269 (1976).
[18]A. A. Minzoni and G. B. Whitham, ''On the excitation of edge waves on beaches,'' J. Fluid Mech. **79**, 273 (1977).
[19]N. Rockliff, ''Finite amplitude effects in free and forced edge waves,'' Math. Proc. Cambridge Philos. Soc. **83**, 463 (1978).
[20]W. Chester, ''Resonant oscillations of water waves. I. Theory,'' Proc. R. Soc. London, Ser. A **306**, 5 (1968).
[21]W. Chester and J. A. Bones, ''Resonant oscillations of water waves. II. Experiment.'' Proc. R Soc. London, Ser. A **306**, 23 (1968).
[22]T. G. Lepelletier and F. Raichlen, ''Nonlinear oscillations in rectangular tanks,'' J. Eng. Mech. **114**, 1 (1988).
[23]D. D. Waterhouse, ''Resonant sloshing near a critical depth,'' J. Fluid Mech. **281**, 313 (1994).
[24]J. R. Ockendon and H. Ockendon, ''Resonant surface waves,'' J. Fluid Mech. **59**, 397 (1973).
[25]O. M. Faltinsen, ''A nonlinear theory of sloshing in rectangular tanks,'' J. Ship Res. **18**, 224 (1974).
[26]O. M. Faltinsen, O. F. Rognebakke, I. A. Lukovsky, and A. N. Timokha, ''Multidimensional modal analysis of nonlinear sloshing in a rectangular tank with finite water depth,'' J. Fluid Mech. **407**, 201 (2000).
[27]C. R. Ruscher, ''The sloshing of trapezoidal reservoirs,'' Ph.D. thesis, University of Southern California, 1999.
[28]C. C. Mei and P. L.-F. Liu, ''The damping of surface gravity waves in a bounded liquid,'' J. Fluid Mech. **59**, 239 (1973).
[29]C. C. Mei, ''The applied dynamics of ocean surface waves,'' Vol. 1 of *Advanced Series on Ocean Engineering* (World Scientific, Singapore, 1989).
[30]R. G. Dean and R. A. Dalrymple, *Water Wave Mechanics for Engineers and Scientists*, Vol. 2 of Advanced Series on Ocean Engineering (World Scientific, Singapore, 1991).
[31]P. R. Garabedian, *Partial Differential Equations* (McGraw-Hill, New York, 1964).
[32]G. H. Keulegan, ''Energy dissipation in standing waves in rectangular basins,'' J. Fluid Mech. **6**, 33 (1959).
[33]C. Martel, J. A. Nicolas, and J. M. Vega, ''Surface-wave damping in a brimful circular cylinder,'' J. Fluid Mech. **360**, 213 (1998).
[34]Z. C. Feng, ''Transition to traveling waves from standing waves in a rectangular container subjected to horizontal excitations,'' Phys. Rev. Lett. **79**, 415 (1997).
[35]M. Abramowitz and I. Stegun, *Handbook of Mathematical Functions*, 9th ed. (Dover, New York, 1972).
[36]P. J. Prince and J. R. Dormand, ''High order embedded Runge–Kutta formulae,'' J. Comput. Appl. Math. **7**, 67 (1981).
[37]C. C. Mei and U. Unluata, ''Harmonic generation in shallow water waves,'' in *Waves on Beaches and Resulting Sediment Transport*, edited by R. E. Meyer (Academic, New York, 1972), pp. 181–202.
[38]O. M. Faltinsen and A. N. Timokha, ''Asymptotic modal approximation of nonlinear resonant sloshing in a rectangular tank with small fluid depth,'' J. Fluid Mech. **470**, 319 (2002).